Fibers and Polymers 2018, Vol.19, No.2, 375-382
DOI 10.1007/s12221-018-7588-7

ISSN 1229-9197 (print version)
ISSN 1875-0052 (electronic version)

Influence of Damping on the Bending and Twisting Modes of Flax Fibre-reinforced Polypropylene Composite

Md Zillur Rahman*, Krishnan Jayaraman, and Brian Richard Mace

Department of Mechanical Engineering, The University of Auckland, Auckland 1142, New Zealand
(Received July 6, 2017; Revised November 23, 2017; Accepted November 27, 2017)

Abstract: The effects of damping on the bending and twisting modes of flax fibre-reinforced polypropylene composites are investigated. The laminate was manufactured by a vacuum bagging process; its dynamic behaviour was then found from the vibration measurements of a beam test specimen using an impulse hammer technique to frequencies of 1 kHz. The frequency response of a sample was measured, and the bending and twisting responses at resonance were used to estimate the natural frequency and loss factor. The single-degree-of-freedom circle-fit method and Newton's divided differences formula were used to estimate the natural frequencies as well as the loss factors. The damping estimates were also investigated using a "carpet" plot. The results show significant variations in loss factors depending on the type of mode. The loss factor generally lies in the range of 1.7-2.2 % for the bending modes, while 4.8 % on average for the twisting modes. Numerical estimates of the response, and in particular the natural frequencies, were made using a Mechanical APDL (ANSYS parametric design language) finite element model, with the beam being discretised into a number of shell elements. The natural frequencies from the finite element analysis show reasonably good agreement (errors < 5 %) with the measured natural frequencies.

Keywords: Composite materials, Flax-polypropylene composites, Damping, Loss factor, Natural frequency

Introduction

Plant fibres are becoming increasingly common as reinforcements in polymer composites. The reduction of available non-renewable resources and the growing concerns for environmental sustainability have directed towards a growing interest in the development of renewable and sustainable plant fibre based composites. Plant fibres are composed of cellulose, hemicellulose, lignin and pectin. These fibres are viscoelastic and hierarchical in nature which contributes to the dissipation of energy [1,2]. Polymers also behave similar to viscoelastic materials and show high damping when compared to metallic materials [3]. Viscoelastic materials have the inherent ability to dissipate energy via converting vibration energy into heat energy during mechanical deformation [4].

Therefore, the embedding of plant fibres into polymeric matrix materials can have multifunctional capabilities [5] such as vibration control, energy dissipation and heat dissipation along with a high stiffness to weight ratio. They can potentially be used in aircraft, aerospace, sporting goods and military applications, where a combination of structural function such as load-bearing and other non-structural function such as vibration damping is of importance.

A number of studies [1,6-11] have been performed to estimate the dynamic behaviour such as natural frequency and loss factor of plant fibre-reinforced polymer composites. Landro and Lorenzo [6,7] examined the dynamic behaviour of plant fibre mat (flax, kenaf and hemp fibres were used in the mat, 50 % by weight) reinforced PP composites at frequencies of up to 4 kHz. An increase in damping with frequency was seen. Kumar *et al*. [8] reported only the first three natural frequencies and the loss factors associated with short sisal and banana fibre-reinforced polyester composites for various fibre lengths (3 mm, 4 mm and 5 mm) and contents (30 %, 40 % and 50 % by weight). They demonstrated that the natural frequencies of the composites are not affected significantly by variations in fibre length. For a constant fibre length (3 mm), two kinds of damping trends were observed with an increase in banana and sisal fibre contents in the case of the first mode: for the former, damping decreases; for the latter, it increases. Assarar *et al*. [9] reported the damping of hybrid-flax reinforced epoxy composites and found that the addition of flax fibre layers outside the carbon laminate enhances its damping significantly. The water uptake increased the loss factor but decreased the bending moduli of quasi-unidirectional flax fibre-reinforced epoxy composites [10]. In another study, Etaati *et al*. [11] reported that the short hemp fibres in the PP matrix create a high amount of interfacial area leading to more energy dissipation. The loss factors also increase with the twist angle of the flax yarns and the crimp in the flax fabrics; this is due to increasing intra-yarn and inter-yarn friction, respectively, as stated in [1].

Some studies [12-15] have shown the effect of damping on the bending and twisting modes particularly for synthetic fibre composites. For example, Berthelot [12] reported the damping of beams (UD (unidirectional) E-glass fibres/epoxy and UD Kevlar fibres/epoxy). The effect of damping on the twisting modes was increased for 0° and 90° fibre oriented samples. This is associated with the increase of in-plane shear deformation of the samples. However, damping was

*Corresponding author: mrah082@aucklanduni.ac.nz

reduced because of the decreased in-plane shear deformation for intermediate fibre orientations (15°, 30°, 45°, 60° and 75°), while for bending modes, high damping of composite beams was seen for these fibre orientations. This is due to the beam bending deformation which acts in the direction transverse to the fibres and in-plane shearing [12,13]. In another study, Hwang and Gibson [14] stated that the impact of damping on the in-plane shear deformation is maximum at 0° fibre orientation. The damping of the transverse bending was slightly higher than those of the longitudinal bending for carbon fibre/epoxy and glass fibre/epoxy composite beams. The damping was much higher in the twisting (as more twisting energy dissipation occurred) mode than in the bending mode [15]. However, the individual bending- and twisting-damping characteristics of plant fibre-based composites have not previously been reported. The present work is, therefore, an attempt to measure the bending and twisting natural frequencies, and the damping associated with them considering a flax/PP composite beam. The quality of the damping estimates from the "carpet" plots is also investigated. In addition, the predicted natural frequencies along with mode shapes are reported to show a comparison with the measured natural frequencies.

Experimental

Materials

Sheets of PP random copolymer (MOPLEN RP241G) with a thickness of 0.38 mm were used as matrix material. The polypropylene sheets were produced by Lyondell Basell Industries and supplied by Field International Ltd., Auckland, New Zealand. The properties of PP are shown in reference [16].

Unidirectional flax fabric (FlaxPly UD180) with a nominal specific weight of 0.18 kg/m^2 and density of 1420 kg/m^3 was used as reinforcement. The flax fabric (4250 yarns/m (warp) and 300 yarns/m (weft)) was supplied by Lineo, Meulebeke, Belgium. The weight distribution of flax fabric in the warp and weft directions was 95.5 % and 4.5 %, respectively. The role of weft (or fill) yarns is to keep the warp yarns in place.

Manufacturing of Composites

Flax fabrics were dried for 24 hours at 70 °C in a vacuum dryer (Squaroid duo-vac vacuum oven) to reduce the moisture content. The vacuum bagging technique was used to manufacture the composite samples. This technique uses atmospheric pressure to hold the laminate in place during the cure cycle. Dry flax fabrics and PP sheets were interleaved by a hand lay-up process and placed on an aluminium plate. A peel ply was then used to separate the breather from the laminate, and the breather was employed to ensure all the air inside the vacuum bag could be drawn into a vacuum port. After sealing the material stack, the air was evacuated from inside the vacuum bag using a vacuum pump. The mould was subsequently placed inside the Elecfurn (FAC 100) oven and heated to a temperature of 190 °C for 1 hour. After this, the mould was cooled to a room temperature of 25 °C. The temperature-pressure cycle (cycle 1) was applied according to reference [17]. The size of the panels was nominally 600 mm×500 mm, with a target thickness, fibre volume fraction and fibre orientation of 3 mm, 0.50 and 0°, respectively. The composite beam sample with the dimension of 350 mm×20 mm×the thickness of the sample was cut from the panel using an automatic saw.

Impact Hammer Technique

An impact hammer technique (IHT) was used to measure the frequency response of the flax/PP sample at an ambient temperature of about 21 °C. One end of the composite beam was clamped to a fixed support and the other end was free to vibrate, as illustrated in Figure 1. The excitation was provided by an impact hammer (PCB model: 086E80) with a soft tip at one point (marked ×), as depicted in Figure 2, and the responses (H_{11}, H_{12}, H_{21}, and H_{22}) were then measured at two locations (marked +) using a laser vibrometer (Polytec model: PDV-100). The resultant frequency responses (H_b and H_t) of bending and twisting modes were estimated using equation (6) and equation (12), respectively. The natural frequencies and loss factors were then extracted from those responses. The data processing was performed in MATLAB [18]. The derivations of resultant bending and twisting frequency responses are described below.

Resultant Bending Response

The resultant displacement at the centre of the beam (see

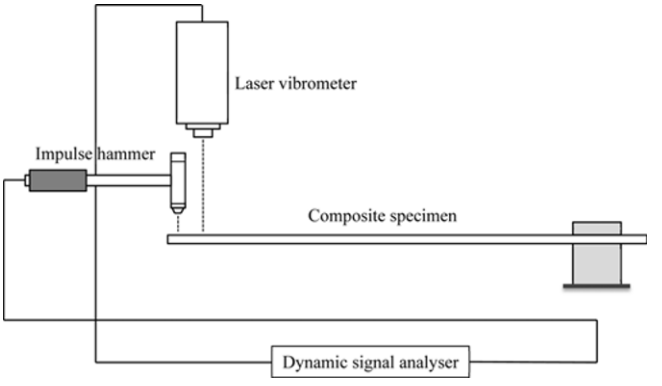

Figure 1. Schematic diagram of experimental setup for an impulse hammer technique.

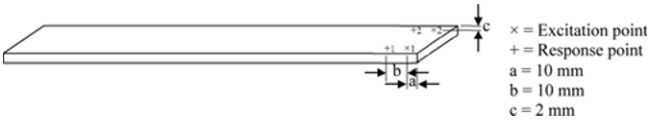

Figure 2. Schematic diagram of the beam for measuring bending and twisting behaviour.

Figure 2)

$$W_r = \frac{W_2 + W_1}{2} \tag{1}$$

where the displacements W_1 and W_2 correspond to the displacements of points 1 and 2, respectively. Forces F_1 and F_2 are applied at points 1 and 2, respectively. In matrix form

$$\begin{bmatrix} W_1 \\ W_2 \end{bmatrix} = \begin{bmatrix} H_{11} & H_{12} \\ H_{21} & H_{22} \end{bmatrix} \begin{bmatrix} F_1 \\ F_2 \end{bmatrix} \tag{2}$$

where H_{ij} is the response at i due to excitation force at j. For bending, the excitation force, $F_1=F_2=F$, equation (2) gives

$$\begin{bmatrix} W_1 \\ W_2 \end{bmatrix} = \begin{bmatrix} H_{11} & H_{12} \\ H_{21} & H_{22} \end{bmatrix} \begin{bmatrix} F \\ F \end{bmatrix} \tag{3}$$

From equation (1) and equation (3)

$$W_r = \frac{W_1 + W_2}{2} = \left(\frac{H_{11} + H_{12} + H_{21} + H_{22}}{2} \right) F \tag{4}$$

Rearranging this equation gives

$$\frac{W_r}{2F} = \frac{H_{11} + H_{12} + H_{21} + H_{22}}{4} \tag{5}$$

The resultant bending frequency response is then

$$H_b = \frac{H_{11} + H_{12} + H_{21} + H_{22}}{4} \tag{6}$$

Resultant Twisting Response

The rotation of the beam (see Figure 2) is

$$\theta = \frac{W_2 - W_1}{D} \tag{7}$$

and the resultant moment is

$$M_r = (F_2 - F_1)\frac{D}{2} \tag{8}$$

where D is the distance between the two response points. For twisting, the excitation force, $F_1=-F$ and $F_2=F$, equation (8) becomes

$$M_r = FD \tag{9}$$

Equation (2) can be written as

$$\begin{bmatrix} W_1 \\ W_2 \end{bmatrix} = \begin{bmatrix} H_{11} & H_{12} \\ H_{21} & H_{22} \end{bmatrix} \begin{bmatrix} -F \\ F \end{bmatrix} \tag{10}$$

From equation (7) and equation (10)

$$\theta = \frac{W_2 - W_1}{D} = \left(\frac{H_{11} + H_{22} - H_{12} - H_{21}}{D^2} \right) (FD) \tag{11}$$

From which the resultant twisting response is

$$H_t = \frac{H_{11} + H_{22} - H_{12} - H_{21}}{D^2} \tag{12}$$

Experimental Modal Analysis

The extraction of modal parameters such as natural frequencies and loss factors from the measured frequency response (i.e., accelerance (acceleration per unit force), see Figure 3(a)) was performed using the single-degree-of-freedom (SDoF) circle-fit method [19]. An illustrative example of this method is shown in Figure 3(b). A portion of the data in a narrow frequency range around each resonance was analysed. A circle was fitted through the use of a least-squares error fit to the data when plotted in the complex plane; the centre and the radius of the circle were estimated. The Newton's divided differences formula was used to determine the location of the natural frequency (ω_r) and its value corresponding to the maximum rate of change of phase [20,21].

The loss factor (η_r) was estimated from the frequency response measurements at frequencies ω_a and ω_b above and below the natural frequency as [19]

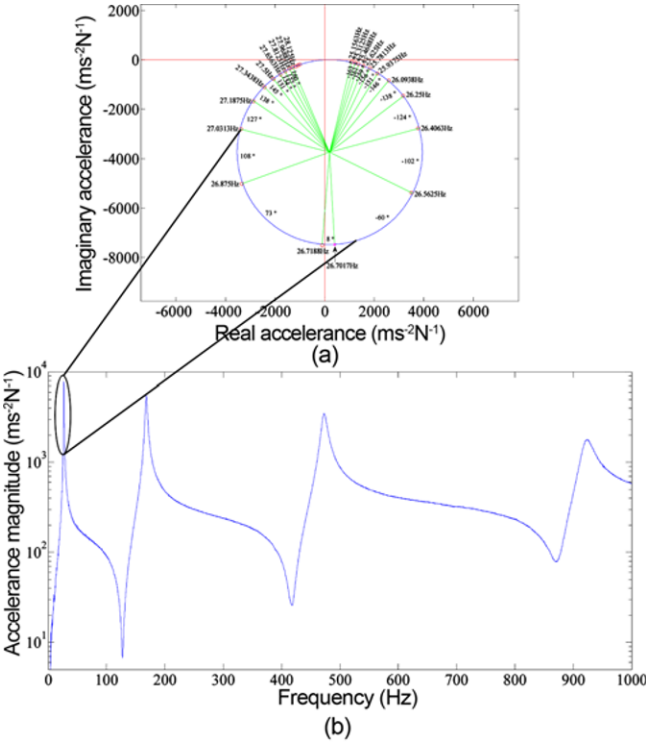

Figure 3. A typical example of (a) magnitude of the measured accelerance and (b) modal circle for extracting natural frequency and loss factor:* Estimated natural frequency (indicated by an arrow) and o discrete frequency data, angles are in degrees.

$$\eta_r = \frac{\omega_a^2 - \omega_b^2}{\omega_r^2\left(\tan\left(\frac{\theta_a}{2}\right) - \tan\left(\frac{\theta_b}{2}\right)\right)} \quad (13)$$

where $\theta_{a,b}$ are the angles between the radii from the centre of the circle to the natural frequency and the frequency response at the chosen frequencies ω_a and ω_b, respectively. The mean loss factors were then calculated from 100 estimates by considering 20 data points, 10 data points below the natural frequency and 10 data points above the natural frequency.

Simulated Modal Analysis

The composite beam was modelled by the finite element program Mechanical APDL [22], and modal analysis was performed. The natural frequencies and mode shapes were then predicted. The beam was considered as a homogenous equivalent shell. The layered element SHELL181 was used. SHELL181 is a 4-node, 3-D shell element with six degrees-of-freedom at each node. The geometry of the composite beam is illustrated in Figure 4.

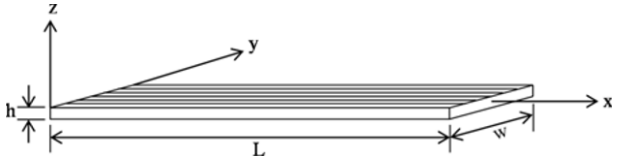

Figure 4. Geometry of the composite beam.

Table 1. Constituents' properties

Materials	Young's modulus (GPa)	Poisson's ratio	Density (kg/m^3)	Reference
Flax fibre	52.28	0.19	1420	[29]
PP	1.10	0.30	900	[29]

Table 2. Elastic properties of the flax/PP composite sample

Properties	Values
Fibre orientation, θ	0 ^{o}
Fibre volume fraction, V_f	0.50
Density (kg/m^3)	1160
Longitudinal modulus, E_1 (GPa)	26.69
Transverse modulus, E_2 (GPa)	3.07
Transverse modulus, E_3 (GPa)	3.07
Shear modulus in-plane 1-2, G_{12} (GPa)	1.21
Shear modulus in-plane 1-3, G_{13} (GPa)	1.21
Shear modulus in-plane 2-3, G_{23} (GPa)	1.13
Major Poisson's ratio in-plane 1-2, ν_{12}	0.23
Major Poisson's ratio in-plane 1-3, ν_{13}	0.23
Major Poisson's ratio in-plane 2-3, ν_{23}	0.36

The composite material was treated as a transversely isotropic linear elastic material, which means that [23-25]

$$E_2 = E_3,\ \nu_{12} = \nu_{13},\ G_{12} = G_{13},\ G_{23} = \frac{E_2}{2(1+\nu_{23})} \quad (14)$$

where E is the elastic modulus, ν is the Poisson's ratio, G is the shear modulus and 1, 2, 3 represent the longitudinal, transverse and out-of-plane directions, respectively, for the orthotropic material. The elastic properties (E_1, E_2, E_3, ν_{12}, ν_{13}, ν_{23}, G_{12}, G_{13} and G_{23}) of the material were predicted using the periodic microstructure model [23,26-29] based on the constituents' Young's moduli and Poisson's ratios, as shown in Table 1. The elastic properties and density of the material are shown in Table 2 and considered as input parameters for the simulation.

A clamped boundary condition at one end of the beam was applied. An automated mesh of 2.5 mm elements was used, producing a model with 960 elements and 1089 nodes. Modes in a frequency range of 0 to 1000 Hz were found using the Block Lanczos method.

Results and Discussion

Damping of Bending Mode

Figure 5 shows the accelerance magnitude for the bending modes of a beam. The resonance peaks are well separated, and the peaks are relatively sharp which indicates that the damping effect is less for the bending. A similar behaviour was also shown in reference [30]. However, the existence of the twisting mode can be seen at a frequency of 274.45 Hz, albeit with a small magnitude. The presence of the twisting mode in the experimentally measured bending response is inevitable because of the inaccuracies in the measurement and manual impact processes, particularly in the precise locations of the excitation and response points. This is also due to small asymmetries of the sample, measurement noise and slight miscalibration.

The natural frequency and loss factor of bending modes and a twisting mode are presented in Table 3. The bending modes have a loss factor of 0.019 on average, whereas the

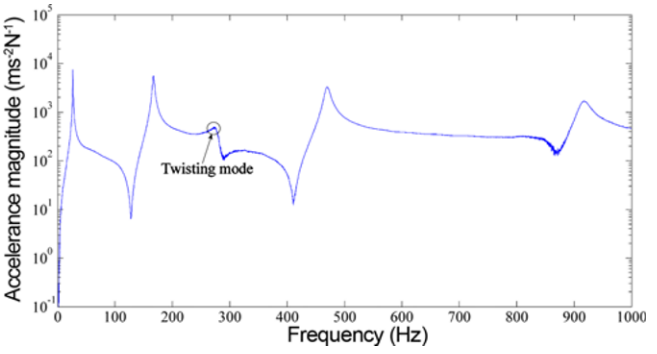

Figure 5. Accelerance magnitude of the flax/PP beam for bending behaviour.

Table 3. Natural frequency and loss factor of the bending and twisting modes

Mode	Mode type	Natural frequency (Hz)	Average loss factor ($\bar{\eta}_r$)	Standard deviation (σ)	Coefficient of variation ($\sigma/\bar{\eta}_r \times 100$ %)	Source
Mode 1	Bending	26.70	0.017	0.0004	2.35 %	Figure 5
Mode 2	Bending	167.00	0.018	0.0001	0.56 %	Figure 5
Mode 3	Twisting	278.05	0.045	0.0022	4.89 %	Figure 6
Mode 4	Bending	469.30	0.020	0.0004	2.00 %	Figure 5
Mode 5	Twisting	859.00	0.050	0.0059	11.80 %	Figure 6
Mode 6	Bending	916.79	0.022	0.0020	9.09 %	Figure 5

twisting mode has a loss factor of 0.045. The loss factor is found to increase 29 % (from 0.017 to 0.022) for frequencies to 1 kHz. The increase in damping with frequency may come from fibre/fibre and fibre/matrix interactions. This trend is consistent with the trend seen by Hong *et al*. in the case of glass fibre- and carbon fibre-reinforced epoxy composite beams [15]. The coefficient of variation of the loss factor estimated at each resonance is in the range of 0.56-9 %.

Damping of Twisting Mode

Figure 6 shows the accelerance magnitude of the measured twisting motion of the beam. There are still bending modes appearing in the measured twisting response. This is again because of the inaccuracies in the measurement process and asymmetry of the sample. The broader resonance peaks are seen for the twisting modes compared to the peaks of the bending modes (see Figure 5), indicating that the damping is greater for such twisting modes. As the composite beam withstands the twisting deformation, more energy dissipation occurs. This results in higher damping in twisting than bending modes. A similar observation of the effect of damping in twisting was reported by Hong *et al*. [15] and Ying *et al*. [31] using glass fibre- and carbon fibre-reinforced epoxy, and carbon fibre-reinforced epoxy composite beams, respectively. The twisting leads to increased damping due to the notable increase of in-plane shear deformation of the specimens [32]. Deformation is predominant in twisting when nodal lines (where the vibration amplitude is zero) cross one another, in which case the polymeric matrix in a composite experiences shearing resulting in significant damping [33]. A significant increase in loss factor of 153 % (from 0.019 to 0.048) is found in the case of the twisting modes.

The natural frequencies and loss factors of twisting and bending modes are shown in Table 3. Noted that the loss factor estimates of the three bending modes are obtained from Figure 5. An increase of 22 % (from 0.045 to 0.050) in loss factor with frequency is observed for twisting modes. The coefficient of variation of the loss factor of twisting modes is higher than the bending modes apart from the highest bending mode, ranging from 5 to 12 %.

Diagnosis of the Quality of the Damping Estimates

The loss factor estimated using equation (13) depends on the chosen frequencies ω_a and ω_b in addition to the estimated natural frequency (ω_r). It is possible to estimate the loss factor (η_r) for any possible combination of ω_a and ω_b. The variation in the individual estimates of loss factor for 100 combinations of the selected frequencies can be seen from the damping "carpet" plots, with two examples shown in Figure 7 and Figure 8. The plots are presented for the first bending and twisting modes, as shown in Figure 5 and Figure 6, respectively. The mean and variance of the estimates are obtained for these 100 estimates. The coefficients of variation of the 100 estimates are 2.35 % (where mean

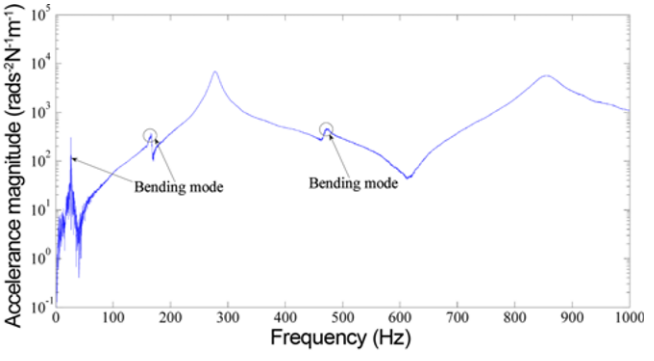

Figure 6. Accelerance magnitude of the flax/PP beam for twisting behaviour.

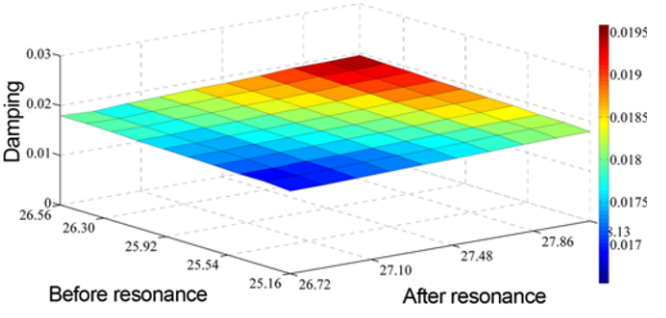

Figure 7. Damping "arpet" plot (beam length: 300 mm, V_f=0.50, θ=0 ° and bending mode 1).

loss factor of 0.017 and standard deviation of 0.0004) and 4.89 % (where mean loss factor of 0.045 and standard deviation of 0.0022) for the first bending and twisting modes, respectively. These are small and indicate that the estimates are of good quality. On the whole, the coefficient of variation is in the range of 0.56-12 %. Relatively large coefficients of variation are observed in the case of the highest modes. In relation to this deviation, some possible measurement errors include errors in excitation and response points, measurement noise, clamping pressure, air damping and non-uniformity in the laminate (voids, variations in thickness and improper bonding).

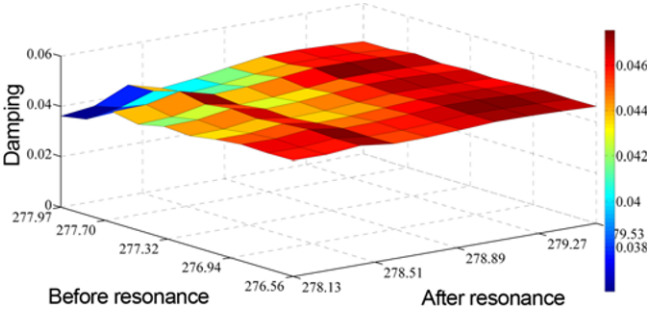

Figure 8. Damping "carpet" plot (beam length: 300 mm, V_f=0.50, θ=0° and twisting mode 1).

Table 4. A comparison between the predicted and measured natural frequencies

Mode	Natural frequency (Hz) (predicted)	Natural frequency (Hz) (measured)	% Error	Mode type
Mode 1	27.74	26.70	-3.76	Out-of-plane bending
Mode 2	167.10	-	-	In-plane bending
Mode 3	173.25	167.00	-3.61	Out-of-plane bending
Mode 4	271.69	278.05	2.34	Twisting
Mode 5	482.46	469.30	-2.73	Out-of-plane bending
Mode 6	828.45	859.00	3.69	Twisting
Mode 7	933.20	-	-	In-plane bending
Mode 8	938.01	916.79	-2.26	Out-of-plane bending

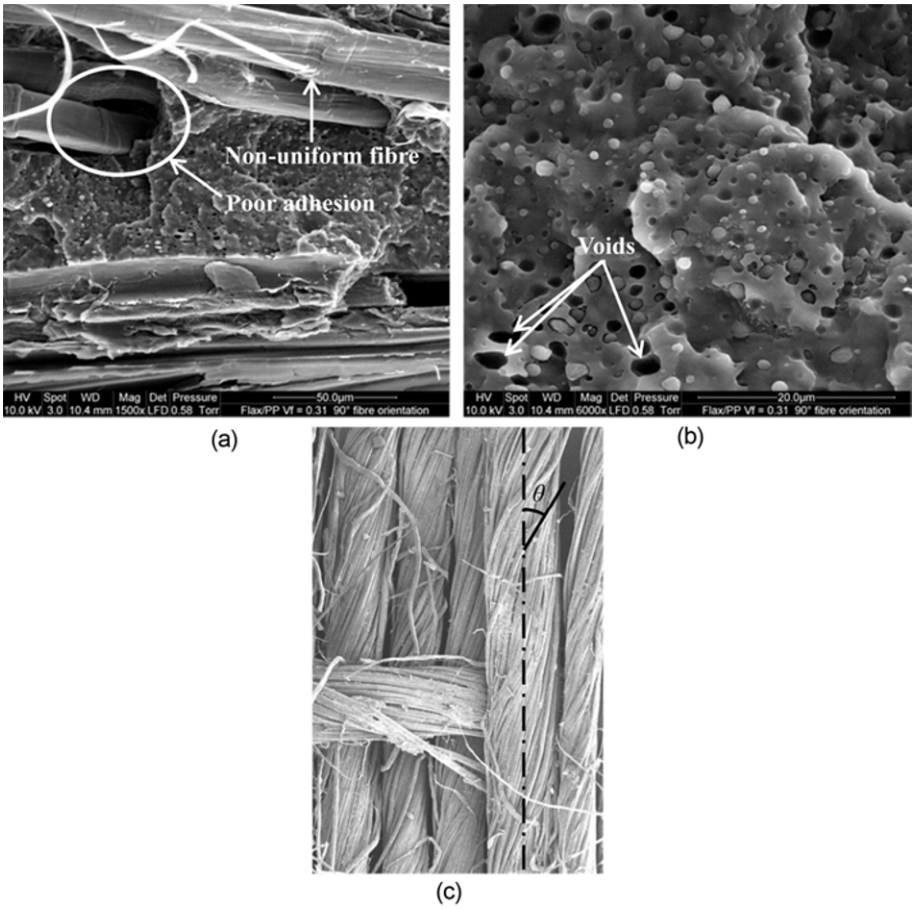

Figure 9. (a) Poor adhesion between flax fibre and PP, (b) voids in a matrix-rich region, and (c) twisted fibres are located helically around the yarn axis.

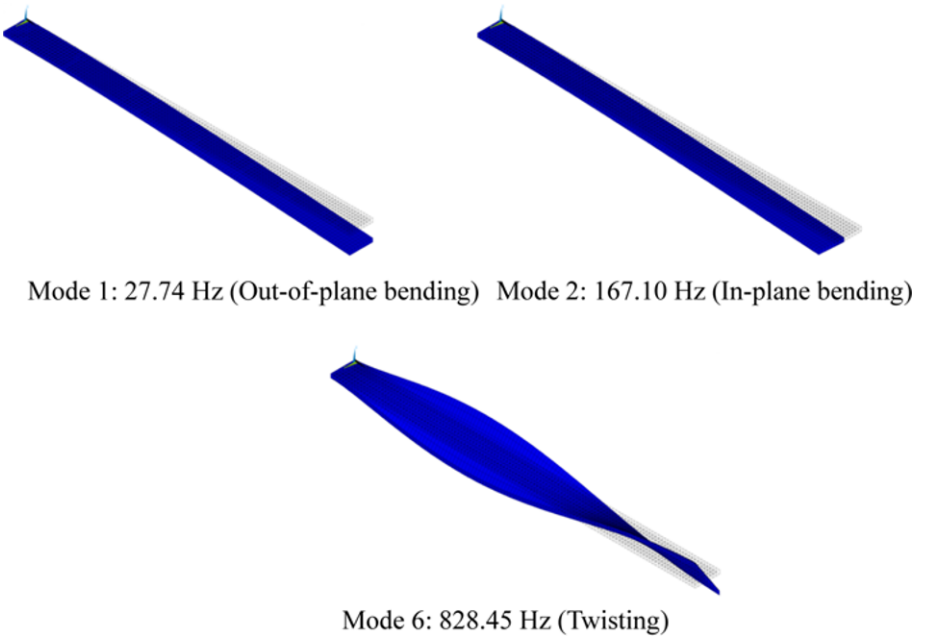

Figure 10. Mode shapes of the flax/PP composite beam.

A Comparison between the Simulated and Measured Natural Frequencies

In Table 4, natural frequencies predicted from the finite element analysis are compared to those obtained by the IHT measurements (see Table 3) of the composite beam. The comparisons are made only for out-of-plane bending and twisting natural frequencies, as only these modes are observed from the IHT measurements. No in-plane bending natural frequency is observed due to the out-of-plane impact load (perpendicular to the top surface of the specimen) and the fact the response is measured in a direction normal to the upper surface of the sample.

The results from the finite element analysis are in general good agreement with the measured natural frequencies, where the maximum error is less than 5 %. The discrepancies between the measured and numerical results may be caused by various reasons such as differences between the actual values of the properties and those assumed in Table 1, noise in the response, variation in the thickness of the composite beam, weak bonding between the matrix and reinforcement (see Figure 9(a)), voids in the specimen (see Figure 9(b)) and other experimental problems such as clamping pressure, transducer effect and air damping. Micrographs of the cross-sections of the specimens were captured using an environmental scanning electron microscope (FEI Quanta 200F, USA). Such factors are not considered throughout the numerical analysis, as the analysis considers the specimen to be perfect with consistent properties, which does not usually happen in practice. Moreover, in the periodic microstructure model and Mechanical APDL, there is no option to consider the twisting of the flax yarns, which is present in the studied flax fabric (see Figure 9(c)).

Three types of mode shapes, out-of-plane bending, in-plane bending and twisting are predicted, as shown in Figure 10, with only out-of-plane bending and twisting being measured.

Conclusion

The effects of damping on the bending and twisting modes of flax/PP composite were estimated from vibration measurements. The SDoF circle-fit method and Newton's divided differences formula were used to estimate the natural frequencies and loss factors of bending and twisting modes. The results show that the damping in the twisting mode is significantly higher (153 %) than the damping in the bending mode. The increase in damping is 29 % over the frequency range of 1 kHz for the bending modes, while the increase is 22 % for the twisting modes. The damping "carpet" plots indicate the quality of the estimates of loss factor. The coefficient of variation of the loss factor estimated at each resonance is in the range of 0.56-12 % irrespective of the mode type. The natural frequencies from the finite element analysis show reasonably good agreement with the measured natural frequencies. However, deviations appear in some instances indicating the need to improve the input material properties data. It can be done by considering a more realistic model simulating twisting of fibres.

Acknowledgements

The first author acknowledges the financial support

provided by the Department of Mechanical Engineering, The University of Auckland, New Zealand.

References

1. F. Duc, P. E. Bourban, and J. A. E. Manson, *Compos. Sci. Technol.*, **102**, 94 (2014).
2. F. Duc, P. E. Bourban, C. J. G. Plummer, and J. A. E. Manson, *Compos. Pt. A-Appl. Sci. Manuf.*, **64**, 115 (2014).
3. D. D. L. Chung, *J. Mater. Sci.*, **36**, 5733 (2001).
4. D. I. Jones, "Handbook of Viscoelastic Vibration Damping", p.7, John Wiley & Sons Ltd., Chichester, West Sussex, England, 2001.
5. R. F. Gibson, *Compos. Struct.*, **92**, 2793 (2010).
6. L. D. Landro and W. Lorenzi, *J. Biobased Mater. Bioenergy*, **3**, 238 (2009).
7. L. D. Landro and W. Lorenzi, *Macromol. Symp.*, **286**, 145 (2009).
8. K. S. Kumar, I. Siva, P. Jeyaraj, J. T. W. Jappes, S. C. Amico, and N. Rajini, *Mater. Des.*, **56**, 379 (2014).
9. M. Assarar, W. Zouari, H. Sabhi, R. Ayad, and J.-M. Berthelot, *Compos. Struct.*, **132**, 148 (2015).
10. K. Cheour, M. Assarar, D. Scida, R. Ayad, and X.-L. Gong, *Compos. Struct.*, **152**, 259 (2016).
11. A. Etaati, S. A. Mehdizadeh, H. Wang, and S. Pather, *J. Reinf. Plast. Compos.*, **33**, 330 (2013).
12. J.-M. Berthelot, *Compos. Struct.*, **74**, 186 (2006).
13. J.-M. Berthelot, M. Assarar, Y. Sefrani, and A. E. Mahi, *Compos. Struct.*, **85**, 189 (2008).
14. S. Hwang and R. Gibson, *J. Mater. Sci.*, **28**, 1 (1993).
15. Y. Hong, X. D. He, R. G. Wang, Y. B. Li, J. Z. Zhang, and H. M. Zhang, *Polym. Polym. Compos.*, **19**, 81 (2011).
16. M. Z. Rahman, K. Jayaraman, and B. R. Mace, *Polym. Compos.*, doi:10.1002/pc.24486 (2017).
17. S. Kazmi, R. Das, and K. Jayaraman, *J. Mater. Process. Technol.*, **214**, 2375 (2014).
18. MATLAB R2013b. The MathWorks Inc., Natick, Massachusetts, 2013.
19. D. J. Ewins, "Modal Testing: Theory, Practice and Application", pp.310-318, Research Studies Press Ltd., Baldock, Hertfordshire, England, 2000.
20. J. Silva and N. Maia, *J. Sound Vib.*, **124**, 13 (1988).
21. N. Maia and J. Silva, "Theoretical and Experimental Modal Analysis", pp.219-227, Research Studies Press Ltd., Baldock, Hertfordshire, England, 1997.
22. ANSYS R16.0. Ansys Inc., Canonsburg, Pennsylvania, 2015.
23. E. J. Barbero, Finite Element Analysis of Composite Materials Using ANSYS®, CRC Press, 2013.
24. R. M. Jones, "Mechanics of Composite Materials", CRC Press, 1998.
25. M. H. Datoo, "Mechanics of Fibrous Composites", Springer, 2012.
26. E. J. Barbero, "Introduction to Composite Materials Design", CRC Press, 2010.
27. R. Luciano and E. Barbero, *J. Appl. Mech.*, **62**, 786 (1995).
28. R. Luciano and E. Barbero, *Int. J. Solids Struct.*, **31**, 2933 (1994).
29. E. Barbero and R. Luciano, *Int. J. Solids Struct.*, **32**, 1859 (1995).
30. M. Z. Rahman, K. Jayaraman, and B. R. Mace, *Fiber. Polym.*, **18**, 2187 (2017).
31. Y. Gao, Y. Li, Y. Hong, H. Zhang, and X. He, *Polym. Polym. Compos.*, **19**, 119 (2011).
32. R. Chandra, S. P. Singh, and K. Gupta, *J. Sound Vib.*, **262**, 475 (2003).
33. R. Adams and M. Maheri, *J. Alloys Compd.*, **355**, 126 (2003).
34. S. M. Panamoottil, Ph. D. Dissertation, The University of Auckland, New Zealand, 2015.